Multiqubit State Tomography with Only a Few Pauli Measurements

Xudan Chai,[1] Teng Ma,[1] Qihao Guo,[2] Zhangqi Yin,[2] Hao Wu,[2] and Qing Zhao[2,*]

[1] *Beijing Academy of Quantum Information Sciences, Haidian District, Beijing 100081, P.R. China*

[2] *Center for Quantum Technology Research and Key Laboratory of Advanced Optoelectronic Quantum Architecture and Measurements (MOE), School of Physics, Beijing Institute of Technology, Beijing 100081, P. R. China*

(Received 22 September 2022; revised 2 June 2023; accepted 4 August 2023; published 18 September 2023)

In quantum information transformation and quantum computation, the most critical issues are security and accuracy. These features, therefore, stimulate research on quantum state characterization. A characterization tool, quantum state tomography, reconstructs the density matrix of an unknown quantum state. Theoretically, reconstructing an unknown state using this method can be arbitrarily accurate. However, this is not so practical owing to the huge burden of measurements and data processing for large numbers of qubits. Even comprising an efficient estimator and a precise algorithm, an optimal tomographic framework can also be overburdened owing to the exponential growth of the measurements. Moreover, the consequential postprocessing of huge amounts of data challenges the capacity of computers. Thus, it is crucial to build an efficient framework that requires fewer measurements but yields an expected accuracy. To this end, we built a tomography schema by which only a few Pauli measurements enable an accurate tomographic reconstruction. Subsequently, this schema was verified as efficient and accurate through numerical simulations on the tomography of multiqubit quantum states. Furthermore, it was proven to be robust through numerical simulations on a noisy superconducting qubit system. Therefore, the tomography schema paves an alternative effective way to reconstruct the density matrix of a quantum state owing to its efficiency and accuracy, which are essential for quantum state tomography.

DOI: 10.1103/PhysRevApplied.20.034039

I. INTRODUCTION

Recent advances in the fundamental research and technological field of quantum physics have been brought about by a surge in theoretical studies on entanglement [1–3], superposition [4], and interference [5], as well as technical improvements in precise quantum manipulations [6] and characterization of quantum circuits [7]. These ongoing studies also stimulate the rapid development of quantum information transformation [8,9], quantum computing [10–14], quantum cryptography [15,16], and quantum simulation [17,18]. In the case of quantum information processing, the issues of greatest concern are the accuracy and security of quantum states. Therefore, considerable attention has been focused on quantum information transformation and quantum computing circuits. Their unit operational blocks are the quantum states on which quantum measurement [19,20] acts and the quantum gates where quantum operations can be performed at specific quantum states. Theoretically, a quantitatively certified quantum state could ensure the accuracy and security of quantum information transformation and quantum computing.

To characterize an unknown quantum state, previous studies have discovered a tool that is a combination of an estimator and a recovery algorithm to reconstruct the density matrix [21,22] of a quantum state with measurements, namely, quantum state tomography [23–28]. These studies involve physical processes with an estimation. Physically, extracting information from quantum states results in a large number of measurements. To postprocess the data obtained requires a valid estimator combined with a recovery algorithm. This framework suffices to theoretically characterize the quantum state precisely. However, tomography encounters a bottleneck when the measurement requirements exponentially increase as qubits multiply. Accordingly, the huge amount of obtained data might overburden the current computer capacity. In practice, it will be technically difficult to accomplish a full tomography larger than 10 qubits. Therefore, a more efficient method that yields high accuracy is required. Efficiency here calls for a constructed estimator, while accuracy also requires a fast and accurate recovery algorithm. Among the common estimators—linear inversion [29], maximum likelihood estimation (MLE) [22,30], Bayesian mean estimation (BME) [31], Fisher information [32] and the self-guided method [33,34], compressed sensing (CS) [35,36]—CS originally played a significant role in the image recovery

*qzhaoyuping@bit.edu.cn

field and then was introduced to quantum state tomography due to its fewer measurement requirements, resulting from compressed sampling. This technique inspired us to reduce the measurement requirements in tomography, as demonstrated in our work. Recovery algorithms also include CVX [32], a two-step descent method, and Nesterov [37], a one-step descent method. Additionally, Powel [38], accelerated proximal gradient (APG) [39], conjugate gradient (CG) [40], and APG-CG [41] have been introduced into the tomography due to their excellent optimizing behaviors.

While the aforementioned studies [42,43] have constructed expected tomographic frameworks that are efficient and accurate, the optimized protocols are preferred, especially for the large-scale qubits system, which paves the way for practical quantum computation and quantum information processing. Here, we construct a tomographic schema that yields high accuracy without overburdened measurement requirements. Although this work is theoretically rooted in the previous work [37] with the estimator, PhaseLift, and the recovery algorithm, Nesterov, this work aims to construct a tomographic schema that requires fewer Pauli measurements [44], especially for some special quantum states that are mostly used in practical quantum computing. The schema has been proven valid and accurate through numerical simulations in multiqubit state tomography. In particular, only measuring two Pauli bases can precisely reconstruct the unknown quantum states without a phase factor [45].

II. METHOD

A. Theoretical analysis

In general, a density matrix for an n-qubit system can be represented by the Stokes parameters,

$$\rho_n = \frac{1}{2^n}\sum_{\mathbf{u}} c_{\mathbf{u}}\sigma_{\mathbf{u}}, \tag{1}$$

in which $c_{\mathbf{u}} \in \mathbb{R}$, $\mathbf{u} = i,j,\ldots,k$ with $i,j,\ldots,k \in \{0,1,2,3\}$ are the Stokes parameters, and $\sigma_{\mathbf{u}} := \sigma_i \otimes \sigma_j \otimes \cdots \otimes \sigma_k$ with $\sigma_{0,1,2,3}$ corresponds to the identity matrix and the Pauli matrices,

$$\sigma_0 := I = \begin{pmatrix} 1 & 0 \\ 0 & 1 \end{pmatrix}, \quad \sigma_1 := \sigma_x = \begin{pmatrix} 0 & 1 \\ 1 & 0 \end{pmatrix},$$
$$\sigma_2 := \sigma_y = \begin{pmatrix} 0 & -i \\ i & 0 \end{pmatrix}, \quad \sigma_3 := \sigma_z = \begin{pmatrix} 1 & 0 \\ 0 & -1 \end{pmatrix},$$

respectively. A Stokes parameter $c_{\mathbf{u}}$ can be obtained using Pauli measurement setting $\mathbf{u}$, where the observable $\sigma_{\mathbf{u}}$ was measured in the tomographic state

$$c_{\mathbf{u}} = \mathrm{tr}(\sigma_{\mathbf{u}}\rho_n) = p_{\mathbf{u}}^{+} - p_{\mathbf{u}}^{-}. \tag{2}$$

Here the probabilities are given by

$$p_{\mathbf{u}}^{\pm} = \sum_{\mathbf{b}} \mathrm{tr}(\mathcal{M}_{\mathbf{u},\mathbf{b}}\,\rho_n), \tag{3}$$

where the summation is over $\left\{\mathbf{b} \,\middle|\, \mathcal{M}_{\mathbf{u},\mathbf{b}}, \text{project onto}, \mathcal{S}_{\mathbf{u}}^{\pm}\right\}$ in which $\mathcal{S}_{\mathbf{u}}^{\pm}$ denote the eigensubspace of $\sigma_{\mathbf{u}}$ corresponding to the eigenvalues ± 1, and $\mathcal{M}_{\mathbf{u},\mathbf{b}}$ denotes a projector of an eigenproduct basis of $\sigma_{\mathbf{u}}$. Note that the subscripts $\{0,1,2,3\}$ in Eq. (1) correspond to I,X,Y,Z measurements, respectively, and we henceforth talk about an X,Y,Z measurement setting rather than a $1,2,3$ measurement setting.

All the diagonal elements of the density matrix can be determined via the Z-direction measurement, which uses σ_z combined with σ_0. All the measurement settings $U\cdots V$ with $U,\ldots,V \in \{X,I\}$ can share a common measurement basis, from which the Stokes parameters $c_{U\cdots V}$ can be obtained from a common set of probabilities. Moreover, for the real part of the density matrix, because all the Stokes parameters with an odd number of Y are zero, only the measurements with an even number of Y are needed. Similarly, for the imaginary part of the density matrix, only the measurements with an odd number of Y are needed.

Based on the aforementioned analysis, we propose the measurement shown in Table I for state tomography for a class of entangled pure states including a Greenberger–Horne–Zeilinger (GHZ), W, and cluster state. For the real part (without a phase factor), a Z-direction measurement is necessary to determine the diagonal elements, and an even number of Y, together with X and Z, direction measurements are used to reconstruct the coherent (off-diagonal) elements. For the imaginary part (off-diagonal), odd numbers of Y together with X and Z are necessary to reconstruct the elements. The specific forms of the measurements shown in Table I are verified through our one- to six-qubit numerical simulations in later sections.

We also propose the general law in Table I to reconstruct the pure or nearly pure state, by considering a multiqubit state with qubit number $n > 6$. The case is simpler when n is even. Here, reconstructing the real parts requires the measurements $X^{\otimes n}$, $Y^{\otimes n}$, and $Z^{\otimes n}$, while $Y^{\otimes n}$ measurements become unnecessary for states without phase factors, that is, all the elements of the density matrix are real. When n is odd, the measurement $Y^{\otimes n-1} \otimes Z$ or $Y^{\otimes n-1} \otimes X$ is required.

As for the limitations of our method, it should be pointed out that the measurements presented in Table I are not sufficient to uniquely determine an arbitrary pure state among all states. It has been proven in [46] that 11 (31) Pauli measurements are needed to uniquely determine an arbitrary

TABLE I. Measurements for reconstructing the density matrices of quantum states of qubits system. The basis measurement law differs between the quantum states with odd $(2m-1)$ and even $(2m)$ numbers of qubits, with $m = \lceil n/2 \rceil$ being the ceiling of $n/2$. Here the stopping condition is MSE $\sim 10^{-2}$. The rightmost column is the number of bases for full tomography [Bases (F)], compared with that for our method [Bases (P)].

qubit	Real part (P)	Imaginary part (P)	Bases (P)	Bases (F)
1	X,Z	Y	3	3
2	XX,ZZ,YY	YZ,ZY	5	9
3	XXX,ZZZ,YYZ	YZZ,ZYZ,ZZY	6	27
4	XXXX,ZZZZ,YYYY	YZZZ,ZYZZ,...,ZYYY,...,YYYZ	11	81
5	XXXXX,ZZZZZ,YYYYZ	YZZZZ,ZYZZZ,... YYYZZ,YYZYZ,...	28	243
6	XXXXXX,ZZZZZZ,YYYYYY	YZZZZZ,ZZZZZY,XXXXXY,YXXXXX,...	135	729
...	...	...	...	...
$2m-1$	$X^{\otimes 2m-1}, Z^{\otimes 2m-1}, Y^{\otimes 2m-2}Z$	$YZ^{\otimes 2m-2}, \ldots, YX^{\otimes 2m-2}, \ldots$	$3 + A^1_{2m-1} + A^3_{2m-1} + \cdots + A^3_{2m-1} + A^1_{2m-1}$	3^{2m-1}
$2m$	$X^{\otimes 2m}, Z^{\otimes 2m}, Y^{\otimes 2m}$	$YZ^{\otimes 2m-1}, \ldots, YX^{\otimes 2m-1}, \ldots$	$3 + A^1_{2m} + A^3_{2m} + \cdots + A^3_{2m} + A^1_{2m}$	3^{2m}

two-qubit (three-qubit) pure state among all states. Moreover, note that the efficiency of the Nesterov recovering algorithm in the next subsection requires the state should be of low rank. We find that, through numerical simulation in Sec. III, the Pauli measurements in Table I can determine the specific states including W, GHZ, and cluster state with high precision and efficiency.

B. Nesterov Recovering algorithm

After framing a schema of measurements using which the density matrices can be reconstructed, an efficient estimator combined with a precise recovering algorithm is mathematically required to solve this problem numerically. Here, we introduce the PhaseLift method [24] as the estimator and the Nesterov algorithm [47] as the recovery core, the validity of which has been demonstrated previously [37]. Integrating this estimator and recovery core allows us to efficiently recover the elements of the density matrix. Based on the method presented in [37], the reconstruction problem can be formulated into a convex optimization problem:

$$\text{minimize}\Bigg\{ \sum_{\mathbf{u},\mathbf{b}} \frac{1}{2}\left[\text{Tr}\left(\mathcal{M}_{\mathbf{u},\mathbf{b}}\,\rho\right) - f_{\mathbf{u},\mathbf{b}}\right]^2 + c_1||\rho||_F^2 + c_2\text{Tr}(\rho)\Bigg\}, \quad \text{subject to } \rho \geq 0, \tag{4}$$

where the relative frequency $f_{\mathbf{u},\mathbf{b}}$ denotes the actual probability of the measurement result of $\mathcal{M}_{\mathbf{u},\mathbf{b}}$, and $c_{1,2}$ represent optimization parameters in the accelerated proximal gradient scheme (APGL) algorithm [48]. In particular, $f_{\mathbf{u},\mathbf{b}}$ is approximately equal to the expected value of $\mathcal{M}_{\mathbf{u},\mathbf{b}}$ when the number of measurements is sufficiently large, c_1 is related to the upper bound of the Lipschitz constant, and c_2 is related to the constrain of the semidefinite property of the density matrix.

The compressed sensing [35] method has been widely used in quantum state tomography, which requires fewer Pauli measurement settings than the full tomographic method. However, the compressed sensing [35] method does not specify which Pauli measurement set can be used.

Previous theoretical research [37] on comparing the performance of other methods (including CVX, APG, and CG) has verified the high accuracy and high speed for state tomography with large numbers of qubits, especially for specific entangled states, such as W state, cluster state, and GHZ state.

Recently, IBM has become a very important quantum computation platform in the cloud. We use this platform to simulate and demonstrate the tomography process. The tomography methods in `qiskit.ignis.verification` of IBM can be categorized into two parts, one designed for reconstructing the density matrix

of the quantum state, and the other for characterizing the performance of a quantum circuit by estimating the average gate fidelity or average error rate. Here we focus on the state tomography in qiskit and we find it includes the MLE and CVX methods. The density matrix reconstruction can be treated to solve the linear problem; we can turn it into an optimization problem by attempting to minimize the problem while subjecting it to additional constraints to ensure it is indeed a density matrix. This is done by $\texttt{state}_{\texttt{cvx fit}}$. Another approach is to solve this optimization problem with no further constraints. The result might not be a density operator, that is, positive semidefinite with trace 1; in this case, the algorithm first rescales in order to obtain a density operator. This is done using $\texttt{state}_{\texttt{mle fit}}$.

Therefore, on this platform, we numerically simulated multiqubit graph state tomography on a noisy superconducting qubit platform in the IBM cloud [49] to explore the robustness of this schema. Specifically, the datum is produced from the simulation on the IBM cloud. Investigations showed that two Pauli measurements enabled us to reconstruct multiqubit states [50].

C. The procedure of the tomographic schema

For the sake of clarity, we will explain this method in detail. The procedure of the simulation method (as shown in Fig. 1) is composed of three steps:

1. Get data through numerical simulation.
2. Process the data obtained Here we feed the data into the estimator [Eq. (4)]. If we want to feed the relative frequency into the estimator, we need to multiply by the corresponding eigenvalues of the state.
3. Execute the Nesterov algorithm, before obtaining the estimated density matrix.

Due to the similarity between this work and the previous one [50], it is necessary to demonstrate the difference between them. First, the numerical simulations in [37] just prove that it is possible to carry out multiqubit state tomography accurately and efficiently in theory, and the Gaussian white noise in those simulations is less practical. Here, we prove the practical possibility of our method by feeding the data obtained from the IBM cloud into the tomographic schema.

Second, we have verified the accuracy and efficiency of the method in [37], which shows that only partially randomly selected Pauli bases produce a highly precise multiqubit tomography. Nonetheless, for a specific quantum state, the bases are not specified. Hence, in this work, we naturally consider that the number of measurement basis might be reduced, especially for some special quantum states, as recent studies have suggested both in theory and experiment [51,52].

In summary, while the previous works have paved the theoretical path, this work uses this method in practice and finds that fewer measurements can produce a precise multiqubit tomography.

III. SIMULATIONS ON TOMOGRAPHY OF MULTIQUBIT QUANTUM STATES

We have theoretically constructed an efficient schema to reconstruct the density matrix of an unknown quantum state by only measuring only a few Pauli bases. Its validity and efficiency were verified through the following simulations on tomography of multiqubit pure states. Figure 2 shows the simulation of the multiqubit GHZ state reconstructions with an efficient tomography schema. In what follows we use the mean square error (MSE), $\mathrm{Tr}\left[(\rho_{\mathrm{E}}-\rho_{\mathrm{T}})'(\rho_{\mathrm{E}}-\rho_{\mathrm{T}})\right]$, and fidelity, $\mathrm{Tr}(\rho_{\mathrm{E}}\rho_{\mathrm{T}})$, to evaluate the accuracy, where ρ_{T} and ρ_{E} denote the target state and the estimated state, respectively. This schema shows higher accuracy and efficiency for the states without phase factors compared with the states with phase factors. Therefore, this method is best suited for the tomography of states that are expected to have no imaginary parts.

According to the above simulations, it is necessary to test this efficient tomography schema for some specific entangled states. Therefore, we use the IBM quantum cloud [49] to simulate the tomography process of quantum states in a superconducting qubit system [53]. Three typical graph states are selected, namely, the W, cluster, and GHZ states, owing to their intensive applications in quantum information and quantum computation. The n-qubit W state and n-qubit GHZ state are expressed as follows:

$$\begin{aligned}|\mathrm{W}\rangle_n &= \frac{1}{\sqrt{n}}\big(|0_1\cdots 0_{n-1}1_n\rangle + |0_1\cdots 0_{n-2}1_{n-1}0_n\rangle \\ &\quad + \cdots + |1_1 0_2\cdots 0_n\rangle\big), \\ |\psi_{\mathrm{GHZ}}\rangle_n &= \frac{1}{\sqrt{2}}\left(|0\rangle^{\otimes n} + |1\rangle^{\otimes n}\right). \end{aligned} \tag{5}$$

We consider the linear-type cluster state, which has the exact form

$$|\mathrm{C}\rangle_n = \frac{1}{2^{n/2}}\bigotimes_{i=1}^{n}\left[|0\rangle_i + |1\rangle_i \otimes \sigma_z^{(i+1)}\right] \tag{6}$$

with the convention $\sigma_z^{(n+1)} \equiv 1$. From Eq. (6), one can have the exact forms of the two-, three-, and four-qubit cluster states:

$$\begin{aligned}|\mathrm{C}\rangle_2 &= (|0+\rangle + |1-\rangle)/\sqrt{2}, \\ |\mathrm{C}\rangle_3 &= (|+0+\rangle + |-1-\rangle)/\sqrt{2}, \\ |\mathrm{C}\rangle_4 &= (|+0+0\rangle + |+0-1\rangle \\ &\quad + |-1-0\rangle + |-1+1\rangle)/\sqrt{2}. \end{aligned}$$

Notably, the two- and three-qubit cluster states are characterized by local unitary equivalence to the GHZ state,

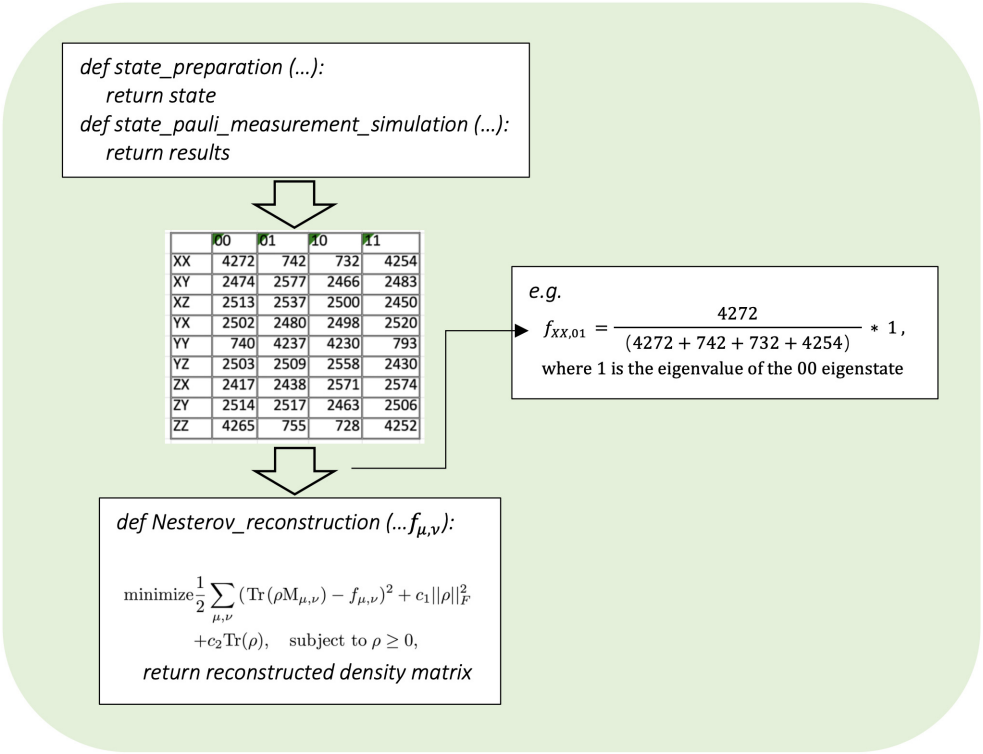

FIG. 1. Schematic diagram for the procedure of the tomographic schema.

whereas any $n > 3$ multiqubit cluster state is not [54]. In a quantum circuit, the cluster state is generated in accordance with its corresponding graph, in which vertices represent qubits with the initial states $|\pm\rangle \equiv (|0\rangle \pm |1\rangle)/\sqrt{2}$, and the edges represent the controlled-phase gates acting on the qubits afterward.

In simulating the real qubit system in practice, we introduce noise models in a quantum circuit. The errors on each quantum gate and the process of reading out are also considered. In particular, we apply a depolarizing channel model to simulate the errors of quantum gates (where the single- and two-qubit gates error rates are set to $a = 0.002$ and $b = 0.005$, respectively). Moreover, statistical noise is very important in quantum computation, and in our simulation, this kind of noise has been modeled with a bit-flip error with a specific probability when the qubits are measured.

Figure 3 shows one- to six-qubit W, cluster, and GHZ state tomography evaluated by MSE and fidelity. Here, we reconstructed density matrices using only two measurement settings, $X^{\otimes n}$ and $Z^{\otimes n}$, with n being the number of qubits. Consequently, our tomography schema, with a smaller MSE and higher fidelity, outperformed the IBM cloud with regard to accuracy. Therefore, this schema might be applied to state certifications for large numbers of qubits. Moreover, the schema showed higher efficiency than the IBM cloud platform. The reconstructed density matrices are shown in Fig. 4.

IV. DISCUSSION ON THE ROBUSTNESS OF THE EFFICIENT TOMOGRAPHY SCHEMA

A comparison between the full tomography and efficient tomography schema is shown in Fig. 5(a). We can

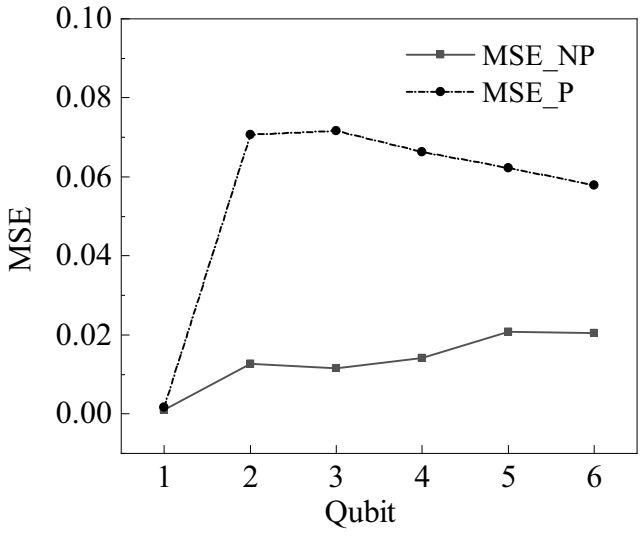

FIG. 2. Schematic for the reconstruction of one- to six-qubit pure states using our efficient tomography schema. The dashed line (MSE_P)and solid line (MSE_NP) represent the states with and without phase factors, respectively.

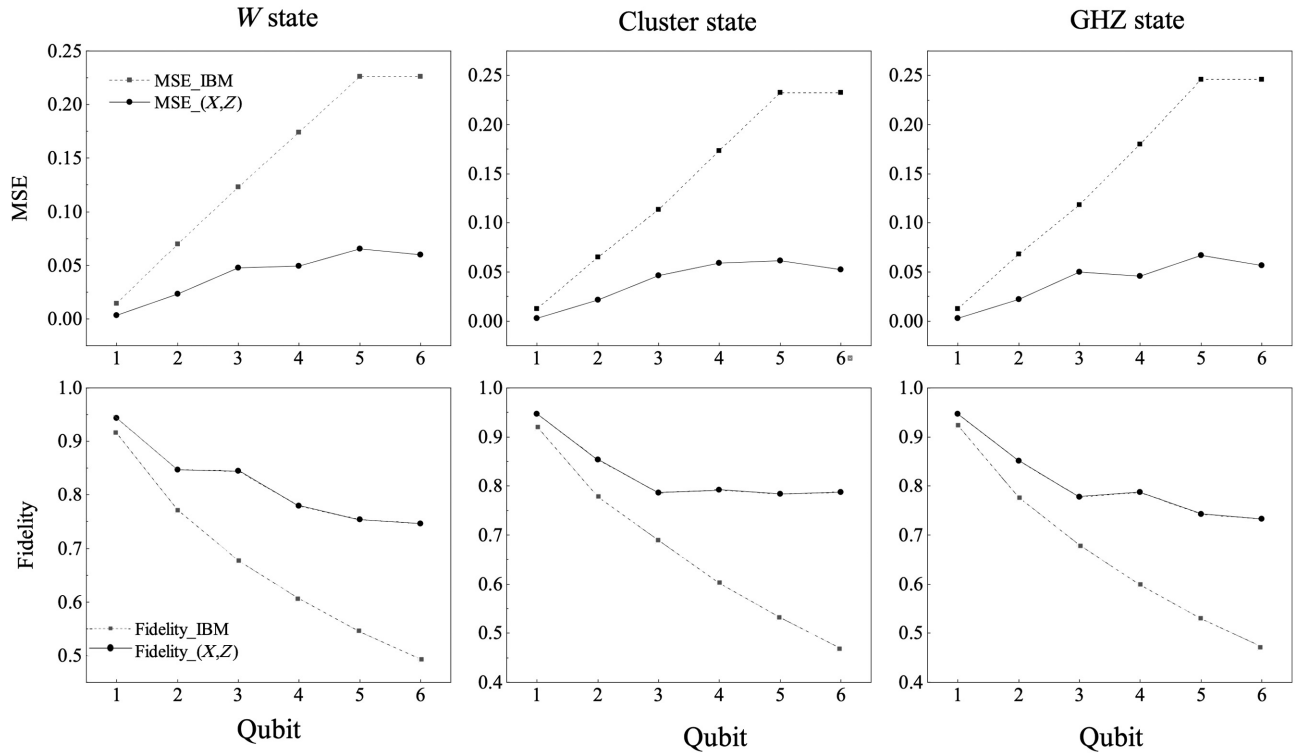

FIG. 3. Tomography simulations for the W, cluster, and GHZ states. The solid lines (MSE, $\text{Fidelity}_{(X,Z)}$) represent our efficient tomography schema, which only measures two directions, X and Z. The dashed lines (MSE/Fidelity IBM) represent the results of the IBM cloud platform. The accuracy and fidelity of the reconstructions are estimated using MSE (shown in the upper and lower panels, respectively).

observe that the number of measurements for the efficient tomography schema increases polynomially, whereas it increases exponentially for the full tomography schema. In particular, in the absence of a phase factor, two measurements can be used for the reconstruction. Evidently, this method outperforms the full tomography schema in terms of efficiency.

A reliable quantum computing and information process requires a precisely controlled qubit system. A qubit system that interacts with its environment at all times easily becomes incoherent, and the noise from the environment technologically challenges the multiplication of the quantum system. Additionally, noise is generated during state preparation and measurement. Therefore, investigating the robustness of the tomography schema under noise for the multiqubit system is essential. Figure 5(b) shows the numerical simulation of multiqubit state tomography for a noisy superconducting qubit system. We investigate the robustness of our tomography schema by varying the two-qubit error rate b from 0 to 0.2 and fixing the single-qubit error rate at $a = 0.002$ as well as the state-of-the-art noise level of the superconducting qubit system. The simulation shows that the noise has a marginal effect on the state tomography as long as the error rate is small enough, where b is less than about 0.08. This type of robustness remains when the number of qubits multiplies. Therefore,

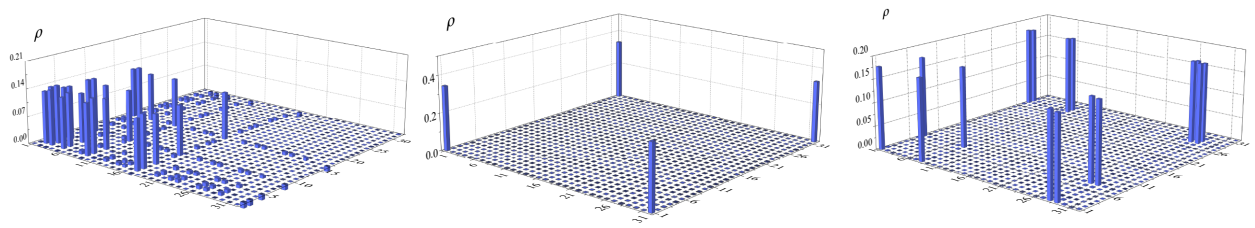

FIG. 4. Populations of density matrices of five-qubit W, cluster, and GHZ states respectively using our efficient tomography schema.

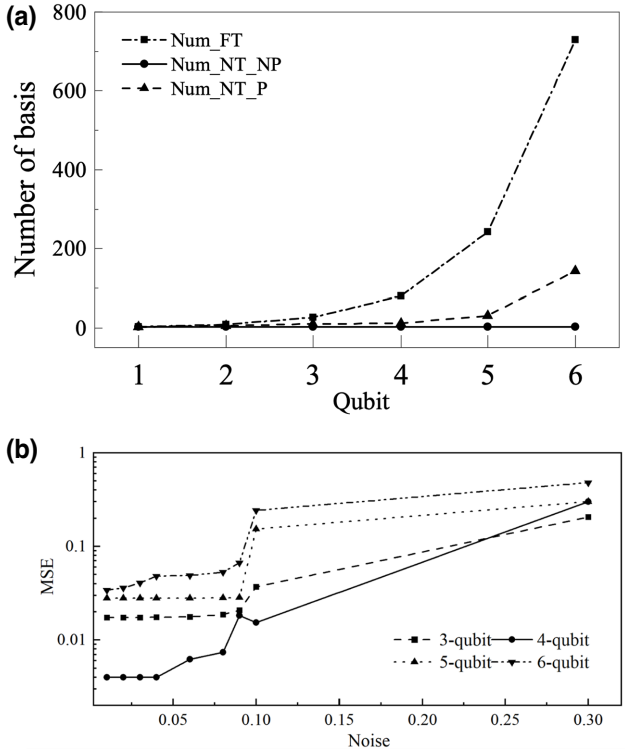

FIG. 5. (a) Comparison between the required measurements of the full tomography and efficient tomography schema. The dash-dotted line (Num_FT), solid line (Num_NT_NP), and dashed line (Num_NT_P) denote the number of measurements with full tomography, efficient tomography schema without a phase, and efficient tomography with a phase, respectively. (b) Robustness of our efficient tomography schema. The horizontal axes represent the noise level of the two-qubit gate.

this schema has promising robustness, even if the scale of qubits grows.

It is worth introducing the new studies within the quantum state tomography field, which has been realized in theory and experiment, respectively [51,52]. The tomographic schema demonstrated by them enables us to accurately determine an unknown quantum state with at most $e^{O(k)}\log^2(n)$ (where n is the number of qubits and k is the number of the disjoint subset), which is realized by concrete measurement protocols. The protocol originates from the theory of perfect hash functions in the field of quantum computation. Using this theory, we can partition the qubits into disjoint subsets, in which we perform all parallel measurements over single-qubit measurement bases (X, Y, or Z), such that all qubits in the same subset have identical measurement settings. This procedure allows us to determine all the reduced density matrices using only $NM3^k$ measurements altogether, where N, M, and k are the number of the partitions, the measurements in an individual base, and the disjoint subsets, respectively. With this theoretic base, the experiment later realizes this theoretic schema in a phonic quantum state reconstruction, using MLE and BME.

In summary, the efficiency and accuracy of the tomography methods in the above studies are mainly guaranteed by efficient measurement protocol instead of an estimator or recovery algorithm. Hence the tomographic schema we put forward here utilizes a different estimator, called PhaseLift, and implements a Nesterov algorithm, which realizes the accuracy and efficiency of tomography.

V. CONCLUSION

We have theoretically framed a tomography schema through which multiqubit states can be reconstructed efficiently and accurately. Physically, the efficiency was ensured by a smaller number of Pauli measurements than required for full tomography. Mathematically, combining the PhaseLift method (as the estimator) and the Nesterov method (as the recovery algorithm) ensured the accuracy of this tomography schema was accurate. Our tomography schema outperformed the full tomography in terms of efficiency and accuracy, particularly in the case of a larger number of qubits, as justified by numerical simulations on the tomography of three entangled states: W, cluster, and GHZ. Considering a quantum state certification that yields a precise estimation with fewer measurements, this efficient tomography schema might be useful in practical quantum computing and information transformation.

ACKNOWLEDGMENT

We would like to thank Dr. Bo Gao at the Beijing Institute of Technology for her careful revision of the manuscript. This work is supported by NSFC Grants No. 11905100 and No. 11675014. Additional support is provided by the Ministry of Science and Technology of China (2013YQ030595-3).

APPENDIX

This segment encompasses “Cloud Quantum Computing Demonstrations” as outlined in the recent announcement.

To address concerns about potential confusion with traditional experiments, it is important to note that the data we obtained from the IBM platform originates solely from simulators. We utilized the *statevector* simulator for ideal quantum states and the *qasm* simulator for data generation.

Although details about the computing device’s layout and characteristics were expected, the tomography process demonstration took place exclusively on IBM’s simulators. Consequently, no additional information was collected during the demonstration. Lastly, statistical analysis was employed to rigorously analyze the simulator-generated dataset on the IBM platform, offering insights into its inherent properties.

[1] H. Ryszard, H. Paweł, H. Michał, and H. Karol, Quantum entanglement, Rev. Mod. Phys. **81**, 2 (2009).

[2] W. Xin and W. M. Mark, Cost of Quantum Entanglement Simplified, Phys. Rev. Lett. **125**, 4 (2020).

[3] T. Zhoudunming, K. Dmitri, and U. Thomas, Einstein-Podolsky-Rosen Paradox and Quantum Entanglement at Subnucleonic Scales, Phys. Rev. Lett. **124**, 6 (2020).

[4] D. Bouwmeester and A. Zeilinger, *The Physics of Quantum Information: Basic Concepts* (Springer, New York City, 2000), p. 1

[5] E. Iliya, R. Alessandro, and G. Yuval, Detection of Quantum Interference without an Interference Pattern, Phys. Rev. Lett. **125**, 2 (2020).

[6] W. E. Carl, P. E. David, and W. J. David, Atom cooling, trapping, and quantum manipulation, Rev. Mod. Phys. **71**, 2 (1999).

[7] K. Martin and R. Ingo, Theory of Quantum System Certification, PRX Quantum **2**, 1 (2021).

[8] N. A. Michael and Chuang Isaac, Quantum computation and quantum information, Am J. Phys. **70**, 5 (2002).

[9] B. Charles, Quantum information and computation, Phys. Today **48**, 10 (1995).

[10] S. S. Gill, A. Kumar, H. Singh, M. Singh, K. Kaur, M. Usman, and R. Buyya, Quantum computing: A taxonomy, systematic review, and future directions, arXiv (2021).

[11] D. P. David, Quantum computation, Science **270**, 255 (1995).

[12] B. Dirk, E. Artur, and Z. Anton, *The Physics of Quantum Information,* (Springer-Verlag, Berlin, 2000), p. 48

[13] B. H. Charles, Quantum information and computation, Nature **404**, 247 (2000).

[14] N. Michael and C. L. Isaac, Quantum computation and quantum information, Phys. Today **54**, 2 (2001).

[15] S. Pirandola, U. L. Andersen, L. Banchi, M. Berta, D. Bunandar, R. Colbeck, D. Englund, T. Gehring, C. Lupo, C. Ottaviani, J. L. Pereira, M. Razavi, J. S. Shaari, M. Tomamichel, V. C. Usenko, G. Vallone, P. Villoresi, and P. Wallden, Advances in quantum cryptography, Adv. Opt. Photon. **12**, 1012 (2020).

[16] B. H. Charles, B. F. B. Gilles, S. Louis, and S. John, Experimental quantum cryptography, J. Cryptol. **5**, 1 (1992).

[17] E. Suguru, S. Jinzhao, L. Ying, B. Simon, and Y. Xiao, Variational Quantum Simulation of General Processes, Phys. Rev. Lett. **125**, 1 (2020).

[18] E. Suguru, S. Jinzhao, L. Ying, B. C. Simon, and Y. Xiao, Quantum simulation, Rev. Mod. Phys. **86**, 1 (2014).

[19] D. F. Walls, M. J. Collet, and G. J. Milburn, Analysis of quantum measurement, Phys. Rev. D **32**, 12 (1985).

[20] J. M. Renes, R. Blume-Kohout, A. J. Scott, and C. M. Caves, Symmetric informationally complete quantum measurements, Math. Phys. **2171**, 2171 (2003).

[21] U. Fano, Description of states in quantum mechanics by density matrix and operator techniques, Rev. Mod. Phys. **29**, 1 (1957).

[22] K. Banaszek, G. M. D'Ariano, M. G. A. Paris, and M. F. Sacchi, Maximum-likelihood estimation of the density matrix, Phys. Rev. A **61**, 1 (1999).

[23] C. Matthias and R. Renato, Reliable Quantum State Tomography, Phys. Rev. Lett. **109**, 12 (2012).

[24] L. Yiping, L. Huan, and Z. Qing, Quantum state tomography and fidelity estimation via Phaselift, Ann. Phys. **360**, 161 (2015).

[25] D. F. V. James, P. G. Kwiat, W. J. Munro, and A. G. White, Measurement of qubits, Phys. Rev. A **64**, 052312 (2001).

[26] J. M Lukens, K. J. H. Law, A. Jasra, and P. Lougovski, A practical and efficient approach for Bayesian quantum state estimation, New J.Phys. **22**, 6 (2020).

[27] G. Stuart and G. Donald, Stochastic relaxation, Gibbs distributions, and the Bayesian restoration of images, IEEE Trans Pattern. Anal. **6**, 6 (1984).

[28] A. B. Joseph, J. R. Evan, and K. G. Paul, Photonic state tomography, Adv. At. Mol. Opt. **52**, 122 (2005).

[29] M. D. Sacchi and T. J. Ulrych, Estimation of the discrete Fourier transform a linear inversion approach, Geophysics **61**, 4 (1996).

[30] F. S. G. Richards, A method of maximum-likelihood estimation, J. R. Stat. Soc. B **23**, 2 (1961).

[31] F. Huszár and N. M. T. Houlsby, Adaptive Bayesian quantum tomography, Phys. Rev. A **85**, 5 (2012).

[32] M. Jian, H. Yi-xiao, W. Xiaoguang, and C. Sun, Quantum Fisher information of the Greenberger-Horne-Zeilinger state in decoherence channels, Phys. Rev. A **84**, 2 (2011).

[33] F. Christopher, Self-Guided Quantum Tomography, Phys. Rev. Lett. **113**, 19 (2014).

[34] C. J. Robert and Ferrie, Experimental Demonstration of Self-Guided Quantum Tomography, Phys. Rev. Lett. **117**, 4 (2016).

[35] G. David, L. Yi-Kai, F. T. Steven, B. Stephen, and E. Jens, Quantum State Tomography via Compressed Sensing, Phys. Rev. Lett. **105**, 15 (2010).

[36] S. T Flammia, D. Gross, Y. Liu, and J. Eisert, Quantum tomography via compressed sensing: Error bounds, sample complexity, and efficient estimators, New J. Phys. **14**, 1367 (2012).

[37] C. Xudan, L. Yi-Ping, Z. Anning, and Z. Qing, Tomographic reconstruction of multiqubit states by phase lift with the Nesterov algorithm, Phys. Rev. A **99**, 4 (2019).

[38] P. Michael, A fast algorithm for nonlinearly constrained optimization calculations, Numer. Anal. **630**, 144 (1978).

[39] L. Huan and L. Zhouchen, Accelerated proximal gradient methods for nonconvex programming, Adv. Neural Inf. Process. Syst. **28**, 1 (2015).

[40] H. Martin, Regularizing properties of a truncated Newton-CG algorithm for nonlinear inverse problems, Numer Func. Anal. Opt. **18**, 971 (1997).

[41] S. Jiangwei, Z. Zhengyun, and N. H. Khoon, Superfast maximum-likelihood reconstruction for quantum tomography, Phys. Rev. A **95**, 6 (2017).

[42] K. Dominik, M. Libor, H. Zdeneek, R. Jaroslav, and S. Luis, Neural-network quantum state tomography, Phys. Rev. A **106**, 1 (2022).

[43] Z. Jingfu, H. S. Swathi, and S. Dieter, Fast Quantum State Tomography in the Nitrogen-Vacancy Center of Diamond, Phys. Rev. Lett. **130**, 9 (2023).

[44] Y. Zhengning, R. Shihao, C. Lianzhen, Z. Nikolay, and G. Weibo, The Pauli matrices in *n* dimensions and finest gradings of simple Lie algebras of type An1, J. Math. Phys. **29** (1988).
[45] Y. Aharonov and J. Anandan, Phase Change during a Cyclic Quantum Evolution, Phys. Rev. Lett. **58**, 16 (1987).
[46] Y. Aharonov and J. Anandan, Pure-state tomography with the expectation value of Pauli operators, Phys. Rev. A **93**, 3 (2016).
[47] S. Becker, J. Bobin, and E. J. Candè, NESTA: A fast and accurate first-order method for sparse recovery, J. Imaging Sci. **4**, 1 (2009).
[48] T. K. Chuan and Y. Sangwoon, An accelerated proximal gradient algorithm for nuclear norm regularized linear least squares problems, Pacific J. Optim. **6**, 615 (2010).
[49] H. Robin and F. Steven, Fault-Tolerant Logical Gates in the IBM Quantum Experience, Phys. Rev. Lett. **122**, 8 (2019).
[50] M. Hein, and J. Eisert, and H. J. Briegel, Multiparty entanglement in graph states, Phys. Rev. A **69**, 062311 (2004).
[51] Y. Zhengning, R. Shihao, C. Lianzhen, Nikolay, and G. Weibo, Experimental Demonstration of Quantum Overlapping Tomography, Phys. Rev. Lett. **130**, 5 (2023).
[52] C. Jordan and W. Frank, Quantum Overlapping Tomography, Phys. Rev. Lett. **124**, 10 (2020).
[53] B. Rami, S. Alireza, L. Lucas, K. Julian, M. Antonio, L. H. Urtzi, B. Ryan, F. G. Austin, C. Brooks, and C. Yu, Digitized adiabatic quantum computing with a superconducting circuit, Nature **534**, 7606 (2016).
[54] H. J. Briegel and R. Robert, Persistent Entanglement in Arrays of Interacting Particles, Phys. Rev. Lett. **86**, 5 (2001).